ELSEVIER

Computers & Geosciences 34 (2008) 1284–1306

COMPUTERS & GEOSCIENCES

www.elsevier.com/locate/cageo

Development of a three-dimensional, regional, coupled wave, current, and sediment-transport model ☆

John C. Warner[a,*], Christopher R. Sherwood[a], Richard P. Signell[a], Courtney K. Harris[b], Hernan G. Arango[c]

[a] *US Geological Survey, Coastal and Marine Geology Program, Woods Hole, MA 02543, USA*
[b] *Virginia Institute of Marine Science, Gloucester Point, VA 23062, USA*
[c] *Institute for Marine and Coastal Sciences, Rutgers-The State University of New Jersey, New Brunswick, NJ 08901, USA*

Received 5 September 2006

Abstract

We are developing a three-dimensional numerical model that implements algorithms for sediment transport and evolution of bottom morphology in the coastal-circulation model Regional Ocean Modeling System (ROMS v3.0), and provides a two-way link between ROMS and the wave model Simulating Waves in the Nearshore (SWAN) via the Model-Coupling Toolkit. The coupled model is applicable for fluvial, estuarine, shelf, and nearshore (surfzone) environments. Three-dimensional radiation-stress terms have been included in the momentum equations, along with effects of a surface wave roller model. The sediment-transport algorithms are implemented for an unlimited number of user-defined non-cohesive sediment classes. Each class has attributes of grain diameter, density, settling velocity, critical stress threshold for erosion, and erodibility constant. Suspended-sediment transport in the water column is computed with the same advection–diffusion algorithm used for all passive tracers and an additional algorithm for vertical settling that is not limited by the CFL criterion. Erosion and deposition are based on flux formulations. A multi-level bed framework tracks the distribution of every size class in each layer and stores bulk properties including layer thickness, porosity, and mass, allowing computation of bed morphology and stratigraphy. Also tracked are bed-surface properties including active-layer thickness, ripple geometry, and bed roughness. Bedload transport is calculated for mobile sediment classes in the top layer. Bottom-boundary layer submodels parameterize wave–current interactions that enhance bottom stresses and thereby facilitate sediment transport and increase bottom drag, creating a feedback to the circulation. The model is demonstrated in a series of simple test cases and a realistic application in Massachusetts Bay.

Keywords: Sediment transport; Nearshore modeling; Three-dimensional numerical model; Model coupling

1. Introduction

1.1. Community modeling approach

Models for transport and long-term fate of particles in coastal waters are essential for a variety of applications related to commerce, defense, public

☆ http://www.unidata.ucar.edu/software/netcdf/.

*Corresponding author. Tel.: +1 508 457 2237; fax: +1 508 457 2310.
E-mail addresses: jcwarner@usgs.gov (J.C. Warner), csherwood@usgs.gov (C.R. Sherwood), rsignell@usgs.gov (R.P. Signell), ckharris@vims.edu (C.K. Harris), arango@marine.rutgers.edu (H.G. Arango).

0098-3004/$ - see front matter © 2008 Elsevier Ltd. All rights reserved.
doi:10.1016/j.cageo.2008.02.012

health, and the quality of the marine environment. There exists a need to develop a sediment-transport model that is freely available, well tested, widely accepted, and applicable to a variety of coastal settings.

We are using a community approach to develop the model as a tool for both research and practical applications. The need and value for this approach was elucidated in a community sediment-transport modeling workshop (Sherwood et al., 2002). A community effort enables us to include a broad range of processes and scales, more than would be feasible for individuals or small groups. We have started with a model that is being used and developed actively by a large research community. We are incorporating proven methodologies from other models such as ECOMSed, EFDC, COHERENS, and Delft3D. Scientists and engineers may contribute to the model according to their expertize, and users (including scientists from other disciplines, students, resource managers, engineers, and operational personnel) may draw from well-tested, state-of-the-art algorithms. Incorporation of alternative parameterizations for similar processes allows us to compare them in identical frameworks. Collaborative work on a community model helps identify key research and modeling issues, and efficiently focus research efforts, minimizing duplication and preventing critical components from being overlooked. Wide use and broad participation in model development, along with extensive testing and peer review, will produce a robust model that can serve the scientific community.

1.2. Regional oceanographic modeling system (ROMS)

Our eventual goal is to produce a sediment model that may be coupled in a flexible way to any of a number of hydrodynamic modules. To reach this goal, we started with a specific model so we could develop sediment-transport algorithms in the context of a completely functional framework. The advancements we are making and the algorithms that we are developing are linked integrally, for now, with the Regional Ocean Modeling System (ROMS). ROMS is a numerical coastal ocean circulation model that includes several submodels that simulate, for example, sea ice, biological processes, and sediment transport. For each application, different components of the model are included or excluded via C-preprocessor (cpp) directives defined in an include file (*cppdefs.h*). This ensures that memory is allocated only as needed, and that only relevant computational algorithms are compiled, creating a more efficient executable file.

The ROMS community interacts through internet, publications, and annual meetings. Revised versions of model code, reports of bugs, and solutions to problems are posted on-line at the ROMS website. Most model inputs and output files, including those relevant for sediment-transport calculations, are written using the NetCDF data architecture (http://www.unidata.ucar.edu/software/netcdf/) in a format compliant with climate and forecast (CF) metadata conventions (http://www.unidata.ucar.edu/software/netcdf/conventions.html). This allows users to capitalize on existing visualization and processing tools that have been and are continuing to be developed by various communities, and encourages documentation of model runs via metadata embedded in input and output files. The code is written in modular Fortran90 and runs in serial mode or on multiple processors using either shared- or distributed-memory architectures (OpenMP or MPI). These characteristics made ROMS an ideal starting point for our development of a community sediment-transport model.

1.3. Objective

This paper describes the implementation in ROMS of a sediment-transport model, new bottom-boundary layer routines, a bed model to track morphology and stratigraphy, wave–current interaction, and coupling of ROMS to the surface wave model Simulating WAves Nearshore (SWAN). The coupled system is distributed as ROMS v3.0. Here we provide background information about ROMS, details of the new sediment algorithms, methods for two-way coupling of ROMS to SWAN, and several examples that demonstrate specific capabilities of the modeling system.

The model is continually evolving, and this description represents a snap-shot of current capabilities and algorithms. Our plan is to eventually extract the sediment-transport components and provide them as separate modules. Our long-term objectives are to expand the modeling system to include effects of cohesive sediments, couple with Boussinesq phase-resolving wave models, add submodels for wave runup on the beach, and include submodels for detailed fluid mechanics and particle interactions near the bed.

2. Circulation and wave model framework

2.1. Hydrodynamic model

ROMS is a three-dimensional, free surface, terrain-following numerical model that solves finite-difference approximations of the Reynolds-averaged Navier–Stokes (RANS) equations using the hydrostatic and Boussinesq assumptions (Chassignet et al., 2000; Haidvogel et al., 2000) with a split-explicit time stepping algorithm (Shchepetkin and McWilliams, 2005; Haidvogel et al., 2007). It uses a horizontal curvilinear Arakawa C grid and vertical stretched terrain-following coordinates (see Section 2). ROMS has a flexible structure that allows choices for many of the model components, including options for advection schemes (second order, third order, fourth order, and positive definite), turbulence submodels, and boundary conditions. It includes bottom- and surface-boundary layer submodels, air-sea fluxes, surface drifters, a nutrient-phytoplankton-zooplankton model, and a fully developed adjoint model for computing model inverses and data assimilation. Momentum, scalar advection, and diffusive processes are represented using transport equations. The density field is determined from an equation of state that accounts for temperature, salinity, and suspended-sediment concentrations. In this paper, the term constant refers to values that are time-invariant, and the term uniform refers to values that do not vary in space. The governing Eqs. (1)–(5) are presented in flux form, in Cartesian horizontal coordinates and sigma vertical coordinates. For curvilinear grids, additional metric terms appear (Haidvogel et al., 2000) that are not shown here. A complete list of variables is given in Table 1. The momentum equations are:

$$\frac{\partial(H_z u)}{\partial t}+\frac{\partial(uH_z u)}{\partial x}+\frac{\partial(vH_z u)}{\partial y}+\frac{\partial(\Omega H_z u)}{\partial s}-fH_z v=-\frac{H_z}{\rho_0}\frac{\partial p}{\partial x}-H_z g\frac{\partial \eta}{\partial x}-\frac{\partial}{\partial s}\left(\overline{u'w'}-\frac{\nu}{H_z}\frac{\partial u}{\partial s}\right)-\frac{\partial(H_z S_{xx})}{\partial x}-\frac{\partial(H_z S_{xy})}{\partial y}+\frac{\partial S_{px}}{\partial s} \quad (1)$$

$$\frac{\partial(H_z v)}{\partial t}+\frac{\partial(uH_z v)}{\partial x}+\frac{\partial(vH_z v)}{\partial y}+\frac{\partial(\Omega H_z v)}{\partial s}+fH_z u=-\frac{H_z}{\rho_0}\frac{\partial p}{\partial y}-H_z g\frac{\partial \eta}{\partial y}-\frac{\partial}{\partial s}\left(\overline{v'w'}-\frac{\nu}{H_z}\frac{\partial v}{\partial s}\right)-\frac{\partial(H_z S_{yx})}{\partial x}-\frac{\partial(H_z S_{yy})}{\partial y}+\frac{\partial S_{py}}{\partial s} \quad (2)$$

$$0=-\frac{1}{\rho_0}\frac{\partial p}{\partial s}-\frac{g}{\rho_0}H_z\rho \quad (3)$$

with continuity as

$$\frac{\partial \eta}{\partial t}+\frac{\partial(H_z u)}{\partial x}+\frac{\partial(H_z v)}{\partial y}+\frac{\partial(H_z \Omega)}{\partial s}=0 \quad (4)$$

and scalar transport:

$$\frac{\partial(H_z C)}{\partial t}+\frac{\partial(uH_z C)}{\partial x}+\frac{\partial(vH_z C)}{\partial y}+\frac{\partial(\Omega H_z C)}{\partial s}=-\frac{\partial}{\partial s}\left(\overline{c'w'}-\frac{\nu_\theta}{H_z}\frac{\partial C}{\partial s}\right)+C_{source} \quad (5)$$

where u, v, and Ω are the mean components of velocity in the horizontal (x and y) and vertical (s) directions respectively; the vertical sigma coordinate $s=(z-\eta)/D$ ranges from $s=-1$ at the bottom to $s=0$ at the free surface; z is the vertical coordinate positive upwards with $z=0$ at mean sea level; η is the wave-averaged free-surface elevation; D is the total water depth $D=h+\eta$; h is the depth below mean sea level of the sea floor; H_z is the grid-cell thickness; f is the Coriolis parameter. An overbar indicates a time average, and a prime ($'$) indicates a fluctuating turbulent quantity. Pressure is p;ρ and ρ_0 are total and reference densities for seawater; g is acceleration due to gravity; ν and ν_θ are molecular viscosity and diffusivity; C represents a tracer quantity (for example, salt, temperature, and suspended-sediment); C_{source} are tracer source/sink terms; and a function $\rho=f(C)$ is required to close the density relation. These equations are closed by parameterizing the Reynolds stresses and turbulent tracer fluxes as

$$\overline{u'w'}=-K_M\frac{\partial u}{\partial z},\quad \overline{v'w'}=-K_M\frac{\partial v}{\partial z},\quad \overline{\rho'w'}=-K_H\frac{\partial \rho}{\partial z} \quad (6)$$

where K_M is the eddy viscosity for momentum and K_H is the eddy diffusivity. Eddy viscosities and eddy diffusivities are calculated using one of five options for turbulence-closure models in ROMS: (i) Brunt-Väisälä frequency mixing in which mixing is based on the stability frequency; (ii) a user-provided analytical expression such as a constant or parabolic shape; (iii) the K-profile parameterization (Large et al., 1994), expanded to include both surface and bottom-boundary layers by Durski et al., 2004; (iv) Mellor-Yamada level 2.5 (MY2.5) method (Mellor and Yamada, 1982); and (v) the generic length-scale (GLS) method (Umlauf and Burchard,

Table 1
List of symbols

Symbol	Description	Dimensions
A_b	Wave orbital excursion amplitude	m
A_R	Wave roller area	m^2
C	Tracer (temperature, salt, or suspended-sediment concentration)	°C, salinity, or $kg\,m^{-3}$
C_{dBF}	Bedform drag coefficient	–
C_{source}	Tracer source/sink term	C units ms^{-1}
D	Total water depth	m
D_{50}	Median grain diameter	m
	Wave energy	$m^3\,s^{-2}$
E_s	Erosion source term	$kg\,m^{-2}\,s^{-1}$
E_0	Erosion rate for each sediment class	$kg\,m^{-2}\,s^{-1}$
F_{CC} F_{CS} F_{SS} F_{SC}	Hyperbolic functions	–
H_z	Grid cell thickness	m
K_H	Eddy diffusivity	$m^2\,s^{-1}$
K_M	Eddy viscosity	$m^2\,s^{-1}$
L	Wave length	m
N	Wave action density	$m^3\,s^{-1}$
N_{bed}	Number of bed layers	–
Q_b	Fraction of breaking waves	–
R_z	Wave roller shape function	–
S_w	Wave energy source/sink term	$m^3\,s^{-2}$
S_{px} S_{py}	Vertically varying vertical radiation stresses	$m^2\,s^2$
S_{xx} S_{xy} S_{yx} S_{yy}	Vertically varying horizontal radiation stresses	$m^2\,s^2$
$\overline{S_{xx}}$ $\overline{S_{xy}}$ $\overline{S_{yx}}$ $\overline{S_{yy}}$	Vertically integrated horizontal radiation stresses	$m^2\,s^2$
T	Near-bottom average wave period	s
T_*	Ratio of $\tau_{wc/\tau ce}$	–
C	Wave celerity	$m\,s^{-1}$
c_x	Wave celerity x-direction	$m\,s^{-1}$
c_y	Wave celerity y-direction	$m\,s^{-1}$
c_g	Wave group celerity	$m\,s^{-1}$
c_θ	Wave celerity in directional (θ) space	$m\,s^{-1}$
c_σ	Wave celerity in frequency (σ) space	$m\,s^{-1}$
c'	Turbulent concentration	°C, salinity, or $kg\,m^{-3}$
d_0	Wave orbital diameter	m
f	Coriolis parameter	s^{-1}
f_w	Wave friction factor	–
g	Gravity	$m\,s^{-2}$
k	Wave number (= 1/wave length)	m^{-1}
k_b	Bottom roughness length	m
k_x	Wave number in x-direction	m^{-1}
k_y	Wave number in y-direction	m^{-1}
k_1 k_2	Active layer thickness coefficients	–
m	Index for each sediment class	–
p	Pressure	$N\,m^{-2}$
q_{bl}	Bedload transport rate	$kg\,m^{-2}\,s^{-1}$
q_{blx}	Bedload transport rate in x-direction	$kg\,m^{-2}\,s^{-1}$
q_{bly}	Bedload transport rate in y-direction	$kg\,m^{-2}\,s^{-1}$
q_{bl_slope}	Bedload slope factor	–
s	Vertical sigma coordinate	–
s	Specific gravity	–
t	Time	s
u	Velocity x-direction	$m\,s^{-1}$
u_b	Bottom orbital velocity	$m\,s^{-1}$
u_*	Friction velocity	$m\,s^{-1}$
u_{*c}	Friction velocity due to currents	$m\,s^{-1}$
u_{*wc}	Friction velocity due to combined waves and currents	$m\,s^{-1}$
u'	Turbulent velocity x-direction	$m\,s^{-1}$
u_s	Vertically varying stokes velocity x-direction	$m\,s^{-1}$

Table 1 (*continued*)

Symbol	Description	Dimensions
$\bar{u}$	Depth-integrated velocity x-direction	$m\,s^{-1}$
$\overline{u_s}$	depth-integrated stokes velocity x-direction	$m\,s^{-1}$
V	Velocity y-direction	$m\,s^{-1}$
v'	Turbulent velocity y-direction	$m\,s^{-1}$
v_s	Vertically varying stokes velocity y-direction	$m\,s^{-1}$
$\bar{v}$	Depth-integrated velocity y-direction	$m\,s^{-1}$
$\overline{v_s}$	Depth-integrated stokes velocity x-direction	$m\,s^{-1}$
w'	Turbulent velocity s-direction	$m\,s^{-1}$
w_s	Sediment settling velocity	$m\,s^{-1}$
x	Horizontal direction	m
y	Horizontal direction	m
z	Vertical elevation	m
z_a	Active layer thickness	m
z_0	Total bottom roughness length	m
z_{oN}	Grain size bottom roughness	m
z_{oST}	Sediment transport bottom roughness	m
z_{oBF}	Bedform bottom roughness	m
z_{oMIN}	Minimum bottom roughness	m
z_r	Reference elevation for BBL	m
Φ	Non-dimensional bedload transport rate	–
$\vec{\Phi}$	Bedload transport vector in direction of and direction perpendicular to currents	–
$\Phi_{\parallel}$	Bedload transport vector in direction of currents	–
$\Phi_{\parallel 1}$, $\Phi_{\parallel 2}$	Bedload transport quantities in direction of currents	–
$\Phi_{\perp}$	Bedload transport vector in direction perpendicular to currents	–
Ω	Vertical velocity s-direction	s^{-1}
α	Roller parameter	–
β	Local bed slope	–
γ	Wave height to water depth ratio	–
γ_w	Wave asymmetry factor	–
γ_1	Linear drag coefficient	–
γ_2	Quadratic drag coefficient	–
δ_{wbl}	Wave boundary layer height	m
η	Wave averaged free surface elevation	m
η_r	Ripple wave height	m
θ	Wave direction	radians
θ_m	Shields parameter (uses τ_m)	
θ_{sf}	Shields parameter (uses τ_{sf})	–
$\theta_{sf\parallel}$	Shields parameter (uses τ_{sf} in direction of currents)	–
$\theta_{sf\perp}$	Shields parameter (uses τ_{sf} in direction perpendicular to currents)	–
$\overrightarrow{\theta_{sf}}$	Shields parameter vector in direction of and direction perpendicular to currents	–
θ_c	Critical shields parameter (uses τ_{ce})	–
$\vec{\theta}$	Directional shields parameter	–
κ	von Kármán's constant (0.41)	–
λ_r	Ripple wave length	m
ρ	Density	$kg\,m^{-3}$
ρ_0	Reference density	$kg\,m^{-3}$
ρ_s	Sediment density	$kg\,m^{-3}$
ρ_{water}	Water density	$kg\,m^{-3}$
ν	Kinematic viscosity	$m^2\,s^{-1}$
ν_θ	Tracer kinematic diffusivity	$m^2\,s^{-1}$
σ	Wave frequency (relative to currents)	s^{-1}
τ_{bx}	Bottom stress x-direction	$m^2\,s^2$
τ_{by}	Bottom stress y-direction	$m^2\,s^2$
τ_c	Bottom stress due to currents alone	$m^2\,s^2$
τ_{ce}	Bottom critical erosion stress	$m^2\,s^2$
τ_m	Mean bottom stress due to combined waves + currents	$m^2\,s^2$
τ_{sx}	Surface stress x-direction	$m^2\,s^2$

Table 1 (*continued*)

Symbol	Description	Dimensions
τ_{sy}	Surface stress y-direction	$m^2 s^2$
τ_{sf}	Total skin friction bottom stress, (maximum combined wave + current)	$m^2 s^2$
τ_{sfm}	Skin friction component due to form drag	$m^2 s^2$
τ_w	Bottom stress due to waves alone	$m^2 s^2$
τ_{wc}	Combined bottom stress due to waves and currents	$m^2 s^2$
ϕ	Sediment bed porosity	–
ϕ_m	Friction angle of sediment	degrees

2003) as implemented by Warner et al. (2005) that also includes the option for surface fluxes of turbulence kinetic energy due to wave breaking. The wide choice in turbulence closures facilitates evaluation of the effects of turbulence parameterizations on model results (for example, see Wijesekera et al., 2003; Li et al., 2005).

We have modified ROMS to include physical processes that are important in nearshore regions by adding radiation-stress terms to the momentum equations based on Mellor (2003, 2005) where a vertical coordinate transformation and phase averaging are used to derive interacting current and surface gravity wave equations. We neglect the momentum transfer term that correlates wind-induced surface pressure fluctuations and wave slope because methods to incorporate these processes are still being developed. The horizontal radiation-stress terms (on the rhs of Eqs. (1) and (2)) are

$$\begin{aligned} S_{xx} &= kE\left[\frac{k_x k_x}{k^2} F_{CS} F_{CC} + F_{CS} F_{CC} - F_{SS} F_{CS}\right] \\ &\quad + \frac{k_x k_x}{k} \frac{c^2}{L} A_R R_z \\ S_{xy} &= S_{yx} = kE\left[\frac{k_x k_y}{k^2} F_{CS} F_{CC}\right] + \frac{k_x k_y}{k} \frac{c^2}{L} A_R R_z \\ S_{yy} &= kE\left[\frac{k_y k_y}{k^2} F_{CS} F_{CC} + F_{CS} F_{CC} - F_{SS} F_{CS}\right] \\ &\quad + \frac{k_y k_y}{k} \frac{c^2}{L} A_R R_z \end{aligned} \tag{7}$$

where the terms in brackets are the traditional momentum flux terms due to the waves (Mellor, 2003, 2005), and the last term is due to the surface roller (Svendsen, 1984; Svendsen et al., 2002), with a vertical distribution expressed as

$$R_z = 1 - \tanh\left(\frac{2s}{\gamma}\right)^4 \tag{8}$$

where R_z vertically distributes the additional stress term due to the roller as an exponentially function decaying with depth and γ is the ratio of wave height to water depth ($\gamma = H_s/D$), H_s is the significant wave height, k is the wavenumber ($k = 2\pi/L$ where L is wavelength), k_x and k_y are the wavenumber components in the x and y directions and c is the wave-propagation speed, computed as

$$c = \frac{\sigma}{k} = \sqrt{\frac{g}{k}\tanh\, kD} \tag{9}$$

where σ is the wave frequency ($\sigma = 2\pi/T$, where T is wave period). The two options available for determining the roller area (A_R) are (1) to obtain A_R directly from the wave model or (2) compute A_R based on a formulation from (Svendsen, 1984):

$$A_R = \frac{\alpha}{\sqrt{2}} H_s L Q_b \tag{10}$$

where α is a parameter with value 0.06, and Q_b is the fraction of breaking waves.

The vertical radiation-stress terms (last term on the rhs of Eqs. (1) and (2)) are:

$$\begin{aligned} S_{px} &= (F_{CC} - F_{SS})\left[\frac{F_{SS}}{2}\frac{\partial E}{\partial x} + F_{CS}(1+s)E\frac{\partial(kD)}{\partial x}\right. \\ &\quad \left. - EF_{SS}\coth(kD)\frac{\partial(kD)}{\partial x}\right] \\ S_{py} &= (F_{CC} - F_{SS})\left[\frac{F_{SS}}{2}\frac{\partial E}{\partial y} + F_{CS}(1+s)E\frac{\partial(kD)}{\partial y}\right. \\ &\quad \left. - EF_{SS}\coth(kD)\frac{\partial(kD)}{\partial y}\right] \end{aligned} \tag{11}$$

where the vertical structure functions in Eqs. (7) and (11) are:

$$\begin{aligned} F_{SS} &= \frac{\sinh(kD(1+s))}{\sinh\, kD} \quad F_{CS} = \frac{\cosh(kD(1+s))}{\sinh\, kD} \\ F_{SC} &= \frac{\sinh(kD(1+s))}{\cosh\, kD} \quad F_{CC} = \frac{\cosh(kD(1+s))}{\cosh\, kD} \end{aligned} \tag{12}$$

and $E = gH_s^2/16$ is the wave energy. The terms in Eqs. (12) provide wave-induced stresses in the momentum equations that decay with depth.

The momentum expressions derived by Mellor (2003, 2005) yield equations with mean (wave-phase averaged) velocities in a Lagrangian reference frame. The Lagrangian and Eulerian reference frames are related by the Stokes velocities u_s and v_s in the x and y directions, computed as

$$u_s = \frac{2k_x}{c}\frac{\cosh 2kD(1+s)}{\sinh 2kD}\left(E + \frac{DgA_R}{L}\right),$$
$$v_s = \frac{2k_y}{c}\frac{\cosh 2kD(1+s)}{\sinh 2kD}\left(E + \frac{DgA_R}{L}\right) \quad (13)$$

where the last terms in the parentheses are the roller contributions. Stokes velocities are subtracted from Lagrangian velocities to maintain a consistent Eulerian reference frame for the entire model dynamics.

ROMS solves the equations with a mode-splitting technique (described in detail by Haidvogel et al., 2007) that requires depth-integrated momentum equations. Including the radiation-stress terms, these are:

$$\frac{\partial(D\bar{u})}{\partial t} + \frac{\partial(\bar{u}D\bar{u})}{\partial x} + \frac{\partial(\bar{v}D\bar{u})}{\partial y} - fD\bar{v} = -D\frac{\partial p}{\partial x} + \tau_{sx} - \tau_{bx} - \frac{\partial \overline{S_{xx}}}{\partial x} - \frac{\partial \overline{S_{xy}}}{\partial y} \quad (14)$$

$$\frac{\partial(D\bar{v})}{\partial t} + \frac{\partial(\bar{v}D\bar{u})}{\partial x} + \frac{\partial(\bar{v}D\bar{v})}{\partial y} + fD\bar{u} = -D\frac{\partial p}{\partial y} + \tau_{sy} - \tau_{by} - \frac{\partial \overline{S_{xy}}}{\partial x} - \frac{\partial \overline{S_{yy}}}{\partial y} \quad (15)$$

and continuity is

$$\frac{\partial \eta}{\partial t} + \frac{\partial(D\bar{u})}{\partial x} + \frac{\partial(D\bar{v})}{\partial y} = 0 \quad (16)$$

where the horizontal radiation-stress terms (Phillips, 1969; Mellor, 2003, 2005) with roller contributions based on Svendsen (1984) and Svendsen et al. (2002) are:

$$\overline{S_{xx}} = E\frac{c_g}{c}\frac{k_x k_x}{k^2} + E\left(\frac{c_g}{c} - \frac{1}{2}\right) + \frac{k_x k_x}{k^2}\frac{c^2 A_R}{L}$$
$$\overline{S_{xy}} = \overline{S_{yx}} = E\frac{c_g}{c}\frac{k_x k_y}{k^2} + \frac{k_x k_y}{k^2}\frac{c^2 A_R}{L}$$
$$\overline{S_{yy}} = E\frac{c_g}{c}\frac{k_y k_y}{k^2} + E\left(\frac{c_g}{c} - \frac{1}{2}\right) + \frac{k_y k_y}{k^2}\frac{c^2 A_R}{L} \quad (17)$$

where the group speed, c_g, is

$$c_g = \frac{\partial \sigma}{\partial k} = \frac{c}{2}\left(1 + \frac{2kD}{\sinh(2kD)}\right) \quad (18)$$

The depth-integrated velocities are also expressed in a Lagrangian reference frame and are related to the Eulerian reference frame by the depth-integrated Stokes velocities $\bar{u}_s$ and $\bar{v}_s$, with:

$$\bar{u}_s = \frac{k_x E}{ckD} + \frac{k_x}{k}\frac{gA_R}{cL}, \quad \bar{v}_s = \frac{k_y E}{ckD} + \frac{k_y}{k}\frac{gA_R}{cL} \quad (19)$$

The Stokes velocities are subtracted from the Lagrangian velocities to maintain a consistent Eulerian reference frame in the model and for the output.

2.2. Wave model

The modification of the momentum equations to include the effects of surface waves requires information on basic wave properties such as wave-energy, propagation direction, and wavelength. Other algorithms, such as the bottom-boundary modules and turbulence submodels may also require wave information such as wave period, bottom orbital velocity, and wave-energy dissipation rate. These quantities are obtained from SWAN (Booij et al., 1999). SWAN is a wave-averaged model that solves transport equations for wave action density N (energy density divided by relative frequency):

$$\frac{\partial N}{\partial t} + \frac{\partial c_x N}{\partial x} + \frac{\partial c_y N}{\partial y} + \frac{\partial c_\sigma N}{\partial \sigma} + \frac{\partial c_\theta N}{\partial \theta} = \frac{S_w}{\sigma} \quad (20)$$

where c_x and c_y are the propagation velocities in the x and y directions, σ is the relative frequency, and θ is the wave direction. SWAN accounts for shoaling and refraction through dependent variations in c_x and c_y. The term S on the right-hand side is a source/sink term representing effects of wind-wave generation, wave breaking, bottom dissipation, and nonlinear wave-wave interactions. SWAN also can account for diffraction, partial transmission, and reflection. Specific formulations for wind input, bottom stress, whitecapping, wave–wave interactions, etc. are described in detail in Booij et al. (2004). SWAN can be run separately and the output used to force the hydrodynamic and sediment routines (one-way coupling). Alternatively, SWAN can be run concurrently with the circulation model with two-way coupling, whereby currents influence

the wave field and waves affect the circulation (see Section 2.4).

2.3. Model domains

ROMS is discretized in horizontal dimensions with curvilinear orthogonal Arakawa *C* grid (Arakawa, 1966) with $\xi(x\text{-})$ and $\eta(y\text{-})$ coordinates (Fig. 1). Grid-cell centers are termed ρ points and are the locations of tracer concentrations, water depth, and sea level. Velocities are computed on the grid-cell faces. The grid can be rectilinear with constant or varying grid spacings, or curvilinear to allow focusing of the mesh to specific areas, for example to accommodate land-sea boundaries. The model also allows land-sea masking to identify regions of dry areas. The model uses a stretched vertical *s*-coordinate system, which are similar to sigma coordinates with additional flexibility: the layers need not be a fixed percentage of the water column (see Haidvogel et al., 2000). Vertical resolution can be adjusted to allow increased resolution near the surface and bottom boundaries. The bed model comprises a user-defined number of layers that extend vertically into the sea floor. See Section 3.2 for a detailed description.

ROMS and SWAN must both use the same grid in our current implementation. The grid may be curvilinear. SWAN depths must coincide with ROMS ρ-points. ROMS has wetting and drying capabilities. The algorithm identify cells with water depths less than a user-specified value, and prevents outward flux of water from those cells, a process called cell flux blocking (Casulli and Cheng, 1992). Flux of water onto cells is always permitted. The same minimum depth can be specified in SWAN to exclude those points during wave computations.

2.4. Model coupling

We used the Model-Coupling Toolkit (MCT; http://www-unix.mcs.anl.gov/mct/; Larson et al., 2005; Jacob et al., 2005) to couple ROMS with SWAN (Warner et al., in press). MCT is an open-source software library, distributed as a set of Fortran90 modules for constructing a coupled model system from individual component models. Each component model has its own grid and runs on its own set of processors. The MCT provides protocols for decomposition and allocation of model grids among different processors, efficient transfer of data fields between the different models,

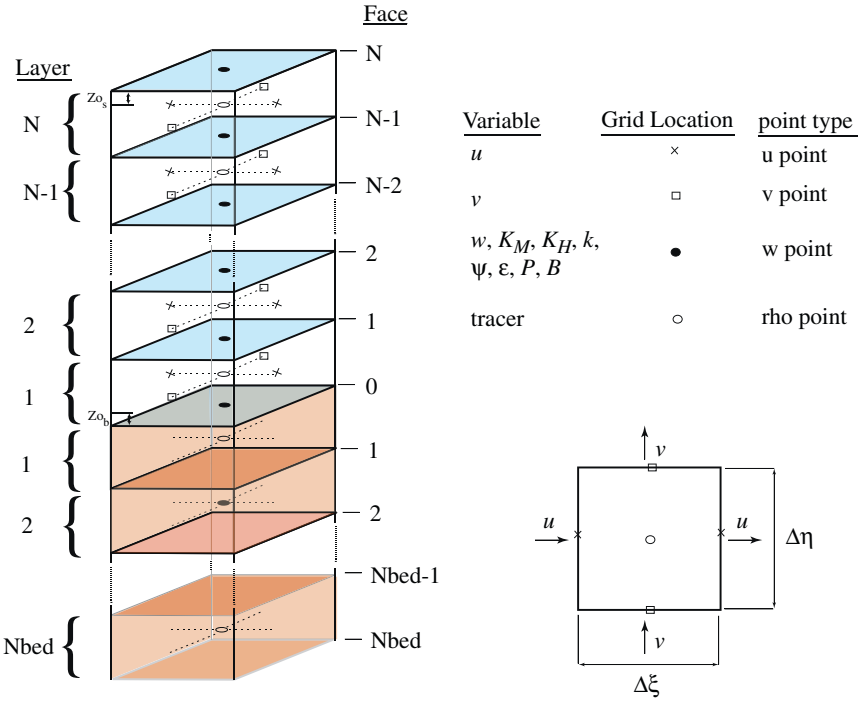

Vertical grid section. Horizontal grid section.

Fig. 1. A vertical section of the ROMS grid showing water column and bed layers.

and interpolation algorithms for the data fields that are transferred. SWAN sends to ROMS arrays of wave height, wavelength, average wave periods at the surface and near the bottom, wave-propagation direction, near-bottom orbital velocity, and wave-energy dissipation rate. ROMS provides to SWAN arrays of water depth, sea-surface elevation, and current velocity. Data exchange between SWAN and ROMS occurs at user-defined synchronization intervals. The frequency of data exchange depends on the application. If the exchanged fields fluctuate rapidly, more frequent synchronization is required. However, data exchange increases run time, so experience is required to determine the optimum synchronization interval for each application.

3. Sediment algorithms and implementation

3.1. Sediment classes

The model is capable of representing an unlimited number of user-defined sediment classes. Each class has fixed attributes of grain diameter, density, settling velocity, critical shear stress for erosion, and erodibility constant. These properties are used to determine bulk properties of each bed layer. Two classes of sediments (non-cohesive and cohesive) are included in the model framework, but the algorithms governing cohesive sediment dynamics are still being developed and are not discussed here.

3.2. Sediment bed

The sediment bed is represented by three-dimensional arrays with a user-specified, constant number of layers beneath each horizontal model cell (Fig. 1). Each cell of each layer in the bed is initialized with a thickness, sediment-class distribution, porosity, and age. The mass of each sediment class in each cell can be determined from these values and the grain density. The age property tracks the time that deposition last occurred in that layer. The bed framework also includes two-dimensional arrays that describe the evolving properties of the seabed, including bulk properties of the surface layer (active-layer thickness, mean grain diameter, mean density, mean settling velocity, mean critical stress for erosion) and descriptions of the subgrid-scale morphology (ripple height and wavelength). These properties are used to estimate bed roughness in the bottom stress calculations. The bottom stresses are then used by the sediment routines to determine resuspension and transport, providing a feedback from the sediment dynamics to the hydrodynamics.

The bed layers are modified at each time step to account for erosion and deposition (Fig. 2) and track stratigraphy. At the beginning of each time step, an active-layer thickness z_a is calculated based on the relation of Harris and Wiberg (1997):

$$z_a = \max[k_1(\tau_{sf} - \overline{\tau_{ce}})\rho_0, \quad 0] + k_2 D_{50} \tag{21}$$

where τ_{sf} is bottom skin-friction stress due to combined maximum wave and current interaction; τ_{ce} is the critical stress for erosion; and the overbar indicates this is averaged over all sediment classes; D_{50} is the median grain diameter of surface sediment; and k_1 and k_2 are empirical constants (values of 0.007 and 6.0, respectively). The thickness of the top bed layer has a minimum thickness equivalent to z_a. If the top layer is thicker than z_a, no action is required. If the top layer is less than z_a thick, then the top layer thickness is increased by entraining sediment mass from deeper layers until the top layer thickness equals z_a. If sediment from deeper than the second layer is mixed into the top layer, the bottom layer is split, enforcing the constant number of layers and conserving sediment mass.

Each sediment class can be transported by suspended-load and/or bedload (described in Sections 3.3 and 3.4). Suspended-load mass is exchanged vertically between the water column and the top bed layer. Mass of each sediment class available for transport is limited to the mass available in the active layer. Bedload mass is exchanged horizontally between the top layers of the bed. Mass of each sediment class available for transport is limited to the mass available in the top layer.

Suspended-sediment that is deposited, or bedload that is transported into a computational cell, is added to the top bed layer. If continuous deposition results in a top layer thicker than a user-defined threshold, a new layer is provided to begin accumulation of depositing mass. The bottom two layers are then combined to conserve the number of layers. After erosion and deposition have been calculated, the active-layer thickness is recalculated and bed layers readjusted to accommodate it. This step mixes away any very thin layer (less than the active-layer thickness) of newly deposited material. Finally the surficial sediment characteristics, such as D_{50}, ripple geometry, etc., are updated and made available to the bottom stress calculations.

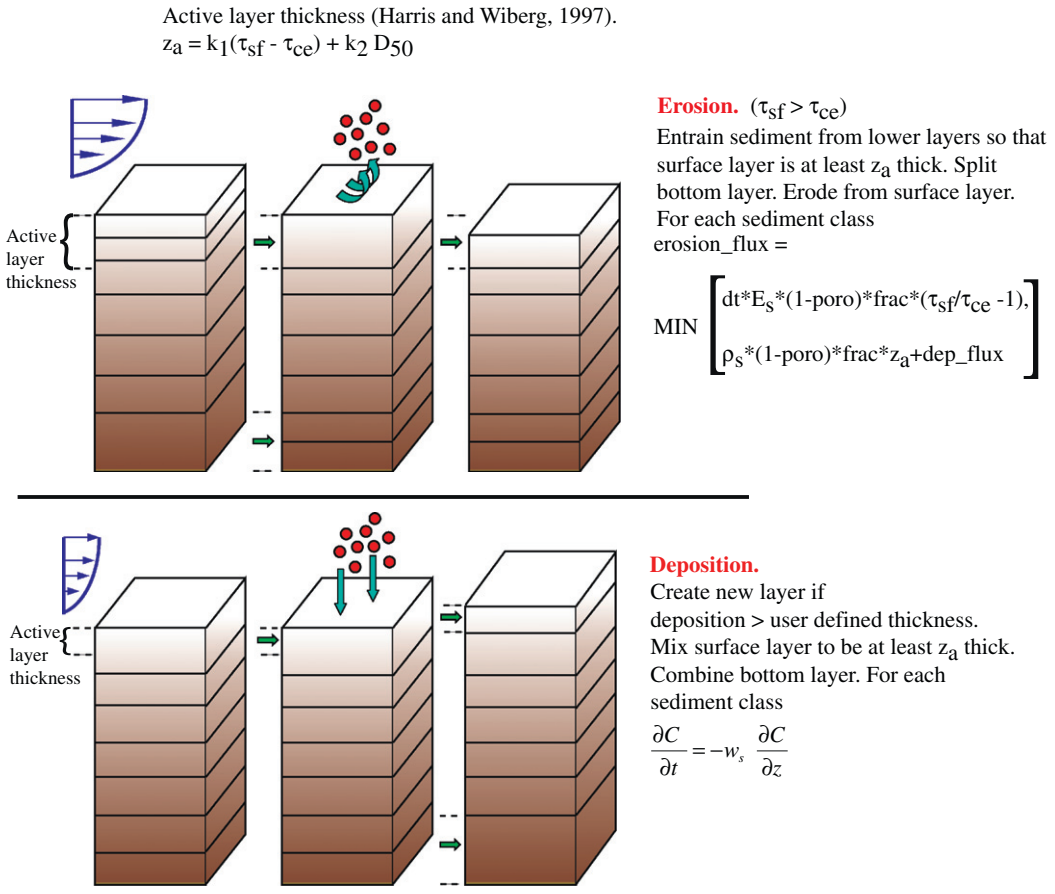

Fig. 2. Distribution of vertical layers in bed model. During erosion top layer thickness is increased to meet active layer thickness. Deposition creates a new layer if timing and thickness criteria are met. Total number of layers must be constant, often requiring a merge or splitting of bottom cells.

3.3. Suspended-sediment transport

Temperature, salinity, and sediment suspended in the water column are transported by solving the advection–diffusion equation (5). However for suspended-sediment, an additional source/sink term is added for vertical settling and exchange with the bed as

$$C_{source,m} = -\frac{\partial w_{s,m} C_m}{\partial s} + E_{s,m} \tag{22}$$

where $w_{s,m}$ is the vertical-settling velocity (positive upwards), $E_{s,m}$ is the erosion source (defined below), and m equals one through the number of classes. The model solves each term of Eq. (5) independently, in the sequence: vertical settling, source/sink, horizontal advection, vertical advection, vertical diffusion, and finally horizontal diffusion. Separation of these calculations has practical advantages because it allows (1) reuse of the routines for advection and diffusion of water-column tracers, (2) use of high-order numerical schemes for vertical settling, and (3) formulation of the flux conditions to ensure conservation of sediment in both bottom sediments and the water column.

The vertical advection algorithm includes a piecewise parabolic method (Colella and Woodward, 1984) and a weighted essentially non-oscillatory (WENO) scheme (Liu et al., 1994). This method integrates depositional flux over multiple grid cells, so it is not constrained by the CFL criterion. Zero-flux boundary conditions are imposed at the surface and bottom in the vertical diffusion equation. The source or sink term in the advection equation represents the net of downward settling and upward flux of eroded material and is only applied to the bottom computational cell. Erosional flux is parameterized following Ariathurai and Arulanandan

(1978) as

$$E_{s,m} = E_{0,m}(1-\phi)\frac{\tau_{sf}-\tau_{ce,m}}{\tau_{ce,m}}, \quad \text{when } \tau_{sf} > \tau_{ce,m} \tag{23}$$

where E_s is the surface erosion mass flux ($\mathrm{kg\,m^{-2}\,s^{-1}}$), E_0 is a bed erodibility constant ($\mathrm{kg\,m^{-2}\,s^{-1}}$), φ is the porosity (volume of voids/total volume) of the top bed layer, and m is an index for each sediment class. The erosional flux for each sediment class is also limited by the availability of that class in the top layer of the bed model.

3.4. Bedload transport

This version of ROMS implements two methods for computing bedload transport: (1) the Meyer-Peter Müeller (1948) formulation for unidirectional flow and (2) the formulae of Soulsby and Damgaard (2005) that accounts for combined effects of currents and waves. The formulae depend on the characteristics of individual sediment classes, including size D, density ρ_s, specific density in water $s = \rho_s/\rho$, and critical shear stress τ_c. Non-dimensional transport rates Φ are calculated for each sediment class and converted to dimensional bedload transport rates q_{bl} using

$$q_{bl} = \Phi\sqrt{(s-1)gD_{50}^3}\rho_s \tag{24}$$

These are horizontal vector quantities with directions that correspond to the combined bed-stress vectors.

3.4.1. Meyer-Peter Müeller

The Meyer-Peter Müeller (1948) formulation is

$$\Phi = \max[8(\theta_{sf}-\theta_c)^{1.5}, \quad 0] \tag{25}$$

where Φ is the magnitude of the non-dimensional transport rate for each sediment class, θ_{sf} is the non-dimensional Shields parameter for skin stress

$$\theta_{sf} = \frac{\tau_{sf}}{(s-1)gD_{50}} \tag{26}$$

$\theta_c = 0.047$ is the critical Shields parameter, and τ_{sf} is the magnitude of total skin-friction component of bottom stress computed from

$$\tau_{sf} = (\tau_{bx}^2 + \tau_{by}^2)^{0.5} \tag{27}$$

where τ_{bx} and τ_{by} are the skin-friction components of bed stress, from currents alone or the maximum wave–current combined stress, in the x and y directions. These are computed at cell faces (u and v locations) and then interpolated to cell centers (ρ points). The bedload transport vectors are partitioned into x and y components based on the magnitude of the bed shear stress as

$$q_{blx} = q_{bl}\frac{\tau_{bx}}{\tau_{sf}}, \quad q_{bly} = q_{bl}\frac{\tau_{by}}{\tau_{sf}} \tag{28}$$

3.4.2. Soulsby and Damgaard

The Soulsby and Damgaard (2005) formulae account for the combined effects of mean currents and asymmetrical waves on bedload flux. Their formulations are based on numerical integration, over a wave cycle, of the non-dimensional transport equation

$$\vec{\Phi} = \max\left[A_2\theta^{0.5}(\theta_{sf}-\theta_c)\frac{\overrightarrow{\theta_{sf}}}{\theta_{sf}}, \quad 0\right] \tag{29}$$

where $\vec{\Phi}$ and $\overrightarrow{\theta_{sf}}$ are vectors with components in the direction of the mean current and in the direction perpendicular to the current, e.g., $\vec{\Phi} = (\Phi_{\parallel}, \Phi_{\perp}), \overrightarrow{\theta_{sf}} = (\theta_{sf\parallel}, \theta_{sf\perp}), \theta_{sf} = |\overrightarrow{\theta_{sf}}|$, θ_c is the critical Shields parameter (i.e. Eq. (26) with τ_{ce}), and $A_2 = 12$ is a semi-empirical coefficient. The implementation of this method requires computation of transport rates in the directions parallel and perpendicular to the currents as

$$\Phi_{\parallel} = \max[\Phi_{\parallel 1}, \quad \Phi_{\parallel 2}] \tag{30}$$

where

$$\Phi_{\parallel 1} = A_2\theta_m^{0.5}(\theta_m - \theta_c) \tag{31}$$

$$\Phi_{\parallel 2} = A_2(0.9534 + 0.1907\cos 2\phi)\theta_w^{0.5}\theta_m + A_2(0.229\gamma_w\theta_w^{1.5}\cos\phi) \tag{32}$$

$$\Phi_{\perp} = A_2\frac{0.1907\theta_w^2}{\theta_w^{3/2} + 1.5\theta_m^{1.5}}(\theta_m \sin 2\phi + 1.2\gamma_w\theta_w \sin\phi) \tag{33}$$

where θ_m is the mean Shields parameter (i.e. Eq. (26) with τ_m) and τ_m is

$$\tau_m = \tau_c\left(1 + 1.2\left(\frac{\tau_w}{\tau_w+\tau_c}\right)^{1.5}\right) \tag{34}$$

and τ_c is the bottom stress from the currents only, τ_w is the bottom stress from the waves only calculated in the bottom-boundary layer routines (see below). The asymmetry factor γ_w is the ratio between the amplitude of the second harmonic and the amplitude of the first harmonic of the oscillatory

wave stress. Following the suggestion of Soulsby and Damgaard (2005), we estimate the asymmetry factor using Stokes second-order theory (e.g., Fredsøe and Deigaard, 1992) and constrain it to be less than 0.2. The non-dimensional fluxes (Eqs. (30) and (33)) are rotated into x and y directions using the directions for mean current and waves and dimensionalized with Eq. (24) to yield values for q_{blx} and q_{bly} for each sediment class.

3.4.3. Bed slope

Computed bedload rates are modified to account for local bed slope following Lesser et al. (2004) with a bed slope term:

$$q_{bl\_slope} = \frac{\tan \varphi_m}{(\tan \varphi_m - \tan \beta)\cos \beta} \tag{35}$$

where the local bed slope $\beta = \tan^{-1}(\mathrm{d}z/\mathrm{d}x_\alpha)$ is evaluated for each direction of transport with a positive value of $\mathrm{d}z/\mathrm{d}x_\alpha$ in the downslope direction, and where φ_m is the friction angle of the sediment (taken as 33°). The bedload magnitudes are then multiplied by q_{bl_slope}.

3.4.4. Bedload numerics

Bedload fluxes are computed at grid-cell centers and limited by the availability of each sediment class in the top layer. Fluxes are translated to cell faces using a simple upwind approach (e.g., Lesser et al., 2004): the bedload flux at each cell face is set to the bedload rate at the upwind cell center. Flux differences are then used to determine changes of sediment mass in the bed at each grid cell.

3.5. Morphology

The bed model accounts for changes in sea floor elevation resulting from convergence or divergence in sediment fluxes. These morphological changes can have significant influence on flow and transport when they are larger than a few percent of the water depth. The morphological changes are accounted for by equating the bottom-boundary condition of the vertical velocity to the rate of change of elevation of the sea floor. This method is completely mass conserving and retains tracer constancy preservation.

A morphological scale factor is also provided to allow an increased rate of morphological change, which can be useful for simulating evolution over long time periods. Strategies for morphological updating are described by Roelvink (2006). In our implementation, bedload fluxes, erosion, and deposition rates are multiplied by a scale factor. A scale factor with a value of one has no effect, and values greater than one accelerate the bed response. For bedload transport, the scale factor is multiplied against the bedload transport rates. For suspended-load transport, the scale factor multiplies the exchange of sediment (erosive or depositional flux) at the bed-water interface. The magnitude of sediment concentrations in the water column are not modified—just the exchange rate to and from the bed. For both bedload and suspended load, sediment is limited in availability as described previously, based on the true amount of sediment mass (not multiplied by the scale factor). This morphological scale factor method works well for systems with unlimited sediment in the bed. However, it can generate extra sediment in systems with limited supplies of bed sediment. This occurs when the amount of sediment to be eroded is limited by the amount available and application of the morphological scale factor cannot remove the scaled amount of sediment from the bed. Subsequent deposition does place a scaled amount of sediment on the bed thus creating new mass in the bed. Other approach (Lesser et al., 2004) is to limit the amount of sediment fluxed to the water column in these situations. This gives unrealistically low sediment concentrations, but conserves bed sediment.

3.6. Sediment density effects

Effects of suspended sediment on the density field are included with terms for the weight of each sediment class in the equation of state for seawater density as

$$\rho = \rho_{water} + \sum_{m=1}^{Nsed} \frac{C_m}{\rho_{s,m}}(\rho_{s,m} - \rho_{water}). \tag{36}$$

This enables the model to simulate processes where sediment density influences hydrodynamics, such as density stratification and gravitationally driven flows.

3.7. Bottom stress calculations

Reynolds stresses, production and dissipation of turbulent kinetic energy, and gradients in velocity and suspended-sediment concentrations vary over short vertical distances, especially near the bed, and

can be difficult to resolve with the vertical grid spacing used in regional-scale applications. ROMS provides algorithms to parameterize some of these subgrid-scale processes in the water column and in the bottom-boundary layer (BBL). Treatment of the BBL is important for the circulation model solution because it determines the stress exerted on the flow by the bottom, which enters the Reynolds-averaged Navier–Stokes equations as a boundary conditions for momentum in the x and y directions:

$$K_M \frac{\partial u}{\partial s} = \tau_{bx}, \quad K_M \frac{\partial v}{\partial s} = \tau_{by} \tag{37}$$

Determination of the BBL is even more important for the sediment-transport formulations because bottom stress determines the transport rate for bedload and the resuspension rate for suspended sediment, as discussed in Sections 3.3 and 3.4.

ROMS implements either of two methods for representing BBL processes: (1) simple drag-coefficient expressions or (2) more complex formulations that represent the interactions of wave and currents over a moveable bed. The drag-coefficient methods implement formulae for linear bottom friction, quadratic bottom friction, or a logarithmic profile. The other, more complex methods, implement some of the many wave–current BBL models (e.g., Jonsson and Carlsen, 1976; Smith, 1977; Grant and Madsen, 1979; Madsen, 1994; Styles and Glenn, 2000) and couple them with calculations of bottom roughness. ROMS offers three methods that implement slightly different combinations of algorithms for the wave–current interactions and moveable bed roughness. The first method (*sg_bbl*) is based on the wave–current algorithm and the ripple geometry and moveable bed roughness of Styles and Glenn (2000, 2002). The second method (*mb_bbl*) uses efficient wave–current BBL computations developed by Soulsby (1995) in combination with sediment and bedform roughness estimates of Grant and Madsen (1982), Nielsen (1986) and Li and Amos (2001). These algorithms and an example of their use on the Southern California continental shelf are described by Blaas et al. (2005). The third method (*ssw_bbl*) implements either the wave–current BBL model of Madsen (1994) or that of Styles and Glenn (2000) along with moveable bed routines proposed by Wiberg and Harris (1994); Harris and Wiberg (2001). The differences in approach among these routines are small, but they can produce significantly different results. After reviewing the simple drag-law approach, we discuss *ssw_bbl* in detail.

The linear and quadratic drag-coefficient methods depend only on velocity components u and v in the bottom grid cell and constant, spatially-uniform coefficients γ_1 and γ_2 specified as input:

$$\tau_{bx} = \left(\gamma_1 + \gamma_2 \sqrt{u^2 + v^2}\right) u \tag{38}$$

$$\tau_{by} = \left(\gamma_1 + \gamma_2 \sqrt{u^2 + v^2}\right) v \tag{39}$$

where γ_1 is the linear drag coefficient and γ_2 is the quadratic drag coefficient. The user can choose between linear or quadratic drag by setting one of these coefficients to zero. The bottom stresses computed from these formulae depend on the elevation of u and v (computed at the vertical mid-elevation of the bottom computational cell). Therefore, in this s-coordinate model, the same drag coefficient will be imposed throughout the domain even though the vertical location of the velocity is different.

The logarithmic formulation assumes that flow in the BBL has the classic vertical logarithmic profile defined by a shear velocity u_* and bottom roughness length z_0 as

$$|u| = \frac{u_*}{\kappa} \ln\left(\frac{z}{z_0}\right) \tag{40}$$

where speed $|u| = \sqrt{u^2 + v^2}$, friction velocity $u_* = \sqrt{|\tau_{bx}| + |\tau_{by}|}$, z is the elevation above the bottom (vertical mid-elevation point of the bottom cell), $\kappa = 0.41$ is von Kármán's constant, and z_0 is a constant (but possibly spatially varying) bottom roughness length (m). Kinematic stresses are calculated as:

$$\tau_{bx} = \frac{\kappa^2 u \sqrt{u^2 + v^2}}{\ln^2(z/z_0)} \tag{41}$$

$$\tau_{by} = \frac{\kappa^2 v \sqrt{u^2 + v^2}}{\ln^2(z/z_0)} \tag{42}$$

The advantage of this approach is that the velocity and the vertical elevation of that velocity are used in the equation. Because the vertical elevation of the velocity in the bottom computational cell will vary spatially and temporally, the inclusion of the elevation provides a more consistent formulation.

More complex routines are required to simulate BBL processes in the presence of waves and mobile sediment. The short (order 10-s) oscillatory shear of wave-induced motions in a thin (a few cm) wave-boundary

layer produces turbulence and generates large instantaneous shear stresses. The turbulence enhances momentum transfer, effectively increasing the coupling between the flow and the bottom and increasing the frictional drag exerted on the mean flow, averaged over many wave periods. The large instantaneous shear stresses often dominate sediment resuspension and enhance bedload transport. Sediment transport can remold the bed into ripples and other bedforms, which present roughness elements to the flow. Bedload transport can also induce drag on the flow, because momentum is transferred to particles as they are removed from the bed and accelerated by the flow. Resuspended sediments can cause sediment-induced stratification and, at high concentrations, change the effective viscosity of the fluid.

The BBL parameterization implemented in ROMS requires inputs of velocities u and v at reference elevation z_r, representative wave-orbital velocity amplitude u_b, wave period T, and wave-propagation direction θ (degrees, in nautical convention). The wave parameters may be the output of a wave model such as SWAN or simpler calculations based on specified surface wave parameters and should represent the full spectrum of motion near the bed (cf. Madsen, 1994; Wiberg and Sherwood, this issue). Additionally the BBL models require bottom sediment characteristics (median grain diameter D_{50}, mean sediment density ρ_s, and representative settling velocity w_s); these are based on the composition of the uppermost active layer of the bed sediment during the previous time step. Bed stresses associated with mean current above the wave-boundary layer τ_b, wave motions τ_w, and maximum vector sum of the two τ_{wc} from the previous time step are used as initial estimates for the next time level.

The procedure for bottom-boundary layer calculations in *ssw_bbl* is as follows:

(1) Ripple height η_r and wavelength λ_r are calculated using information from the previous time step and the Malarkey and Davies (2003) implementation of the Wiberg and Harris (1994) formulation, which is valid for wave-dominated conditions. They approximate ripple wavelength as $535D_{50}$ and ripple steepness as

$$\frac{\eta_r}{\lambda_r} = \exp\left[-0.095\left(\ln\left(\frac{d_0}{\eta_r}\right)\right)^2 + 0.442\left(\ln\left(\frac{d_0}{\eta_r}\right)\right) - 2.28\right] \quad (43)$$

where $d_0 = u_b T/\pi$ is the wave-orbital diameter. When transport stage is below the threshold for sediment transport ($T_* = \tau_{wc}/\tau_{ce} < 1$), ripple dimensions from the previous time step are retained.

(2) Roughness lengths associated with grain roughness z_{0N}, sediment transport z_{0ST}, and bedform roughness length (ripples) z_{0BF} are estimated as

$$z_{0N} = 2.5D_{50}/30 \quad (44)$$

$$z_{0ST} = \alpha D_{50}\, a_1 \frac{T_*}{1 + a_2 T_*} \quad (45)$$

$$z_{0BF} = a_r \eta_r^2/\lambda_r \quad (46)$$

where the sediment-transport coefficients are $\alpha = 0.056$, $a_1 = 0.068$, and $a_2 = 0.0204\ln(100D_{50}^2) + 0.0709\ln(100D_{50})$ (Wiberg and Rubin, 1989) with the bedform roughness D_{50} expressed in meters, and where a_r is a coefficient that may range from 0.3 to 3 (Soulsby, 1997). Grant and Madsen (1982) proposed $a_r = 27.7/30$ but we use as a default value $a_r = 0.267$ suggested by Nielsen (1992). The roughness lengths are additive, so subsequent BBL calculations use $z_0 = \max[z_{0N} + z_{0ST} + z_{0BF}, \quad z_{0MIN}]$, where z_{0MIN} allows setting a lower limit on bottom drag (default $z_{0MIN} = 5\mathrm{e}^{-5}$ m).

(3) Initial estimates of (kinematic) bottom stresses based on pure currents τ_c ($= \tau_b$) and pure waves τ_w ($\tau_b = 0$) are made as follows.

$$\tau_c = \frac{(u^2 + v^2)\kappa^2}{\ln^2(z/z_0)} \quad (47)$$

and $\tau_w = 0.5 f_w u_b^2$, where f_w is the Madsen (1994) wave-friction factor, which depends on the ratio of the wave-orbital excursion amplitude to the bottom roughness length A_b/k_b, where $A_b = u_b T/(2\pi)$ and $k_b = 30z_0$:

$$f_w = \left\{ \begin{array}{cc} 0.3, & A_b/k_b \leqslant 0.2 \\ \exp(-8.82 + 7.02(A_b/k)^{-0.078}), & 0.2 < A_b/k_b \leqslant 100 \\ \exp(-7.30 + 5.61(A_b/k)^{-0.109}), & A_b/k_b > 100 \end{array} \right\} \quad (48)$$

(4) The pure currents and pure wave limits are used as initial estimates for calculations towards consistent profiles for eddy viscosity and velocity between z_0 and z_r, using either the model of Madsen (1994) or Styles and Glenn (2000). Both

of these models assume eddy viscosity profiles scaled by $u_{*wc} = \sqrt{\tau_{wc}}$in the wave-boundary layer (WBL) and $u_{*c} = \sqrt{\tau_b}$ in the current boundary layer, calculated as

$$K_M = \begin{cases} \kappa u_{*wc} z, & z < \delta_{wbl} \\ \kappa u_{*c} z, & z > \delta_{wbl} \end{cases} \quad (49)$$

where δ_{wbl} is the thickness of the WBL, which scales as $u_{*wc}T/(2\pi)$. τ_{wc} represents the maximum vector sum of wave- and current-induced stress, but the τ_b is influenced by the elevated eddy viscosity in the WBL, and must be determined through an iterative process. The shape and elevation of the transition between these profiles and other details differ among the two models, but both the models of Madsen (1994) or Styles and Glenn (2000) return values for the horizontal vectors τ_b, τ_w, and τ_{wc}. The parameter τ_b is the mean (over many wave periods) stress used as the bottom-boundary condition in the momentum equations, and τ_{wc} is the maximum instantaneous stress exerted over the bottom by representative waves and currents.

(5) When ripples are present, τ_{wc} is a combination of form drag, which does not directly contribute to sediment transport, and skin friction, which does. The next step in the BBL calculations is to estimate the skin-friction component of τ_{wc} using the ripple dimensions and a bedform drag-coefficient approach (Smith and McLean, 1977; Wiberg and Nelson, 1992), as follows.

$$\tau_{sfm} = \tau_{wc}\left[1 + 0.5 C_{dBF}\frac{\eta_r}{\lambda_r \kappa^2}\left(\ln\frac{\eta_r}{(z_{0N} + z_{0ST})} - 1\right)^2\right]^{-1} \quad (50)$$

where $C_{dBF} \approx 0.5$ is a bedform drag coefficient for unseparated flow (Smith and McLean, 1977).

(6) Finally, because shear stress varies between ripple crests and troughs, an estimate of the maximum shear stress at the crests τ_{sfm} is calculated for use in sediment-transport algorithms as

$$\tau_{sf} = \tau_{sfm}\left(1 + 8\frac{\eta_r}{\lambda_r}\right) \quad (51)$$

In summary, the more advanced BBL routines calculate current and wave-boundary layer bottom stresses under the combined influence of wave, currents, and mobile sediments. These stresses directly influence flow near the bottom and act as agents for sediment resuspension and bedload transport.

4. Examples

In this section we provide four examples that highlight the capabilities of the sediment-transport model. Example 1 demonstrates the ability of the model produce a classic suspended-sediment profile and illustrates the effect of varying vertical grid resolution and turbulence submodels. Example 2 demonstrates the morphology component of the model in a simulation of a lab experiment with a migrating trench. Example 3 demonstrates the impact of dynamic coupling for wave–current interactions at a tidal inlet. Example 4 is a realistic application with complex bathymetry that demonstrates transport and sorting of multiple sediment classes.

4.1. Example 1: Steady uniform open-channel flow

Example 1 exercises the models ability to simulate vertical profiles of suspended-sediment concentrations (no bedload) with varying vertical grids and turbulence closures. The simulation represents suspended-sediment transport for steady horizontally uniform flow in a straight rectangular channel, modified slightly from Warner et al. (2005). The channel is placed on a constant slope of 4×10^{-5} m/m and a depth-mean velocity of $1\,\mathrm{m\,s^{-1}}$ is imposed at both the upstream and downstream ends. The water-surface elevation is allowed to vary along the length of the channel. Radiation conditions for the free surface and 3D momentum at both ends allow waves to propagate out of the domain. An unlimited supply of sediment is available in the bed. Additional details are listed in Table 2.

Numerical simulations of vertical suspended-sediment profiles can be sensitive to the number and placement of vertical grid levels. As the number of vertical grid levels increases, the gradient of suspended-sediment near the bed is better resolved. Effects of changing the number of vertical levels and resolution are evaluated using the k–ε turbulence closure. The number of vertical levels is varied with values of 10, 20, 40, and 80 evenly spaced cells, and 10 and 20 cells using the stretching parameters of $\theta_s = 3$, $\theta_b = 1$, and $T_{cline} = 0$ (see Haidvogel et al., 2000). Vertical profiles of suspended-sediment converge with 40 or more evenly spaced cells (Fig. 3).

Table 2
Model parameters for test case 1—open-channel flow

Model parameter	Variable	Value
Length, width, depth	*Xsize*, *Esize*, *depth*	10 000, 100, 10 m
Number of grid spacings	*Lm*, *Mm*, *Nm*	100, 10, 20 (+variable)
Bottom roughness	*Zob*	0.0053 m
Time step	*dt*	30 s
Simulation steps	*Ntimes*	5000
Settle velocity	w_s	$1.0\,\mathrm{mm\,s^{-1}}$
Erosion rate	E_0	$5\times10^{-5}\,\mathrm{kg\,m^{-2}\,s^{-1}}$
Critical stresses	τ_{ce}	$0.05\,\mathrm{N\,m^{-2}}$
Porosity	φ	0.90
Bed slope	S_0	4×10^{-5}
Inflow/outflow boundary condition	$\bar{u}$	$1\,\mathrm{m\,s^{-1}}$

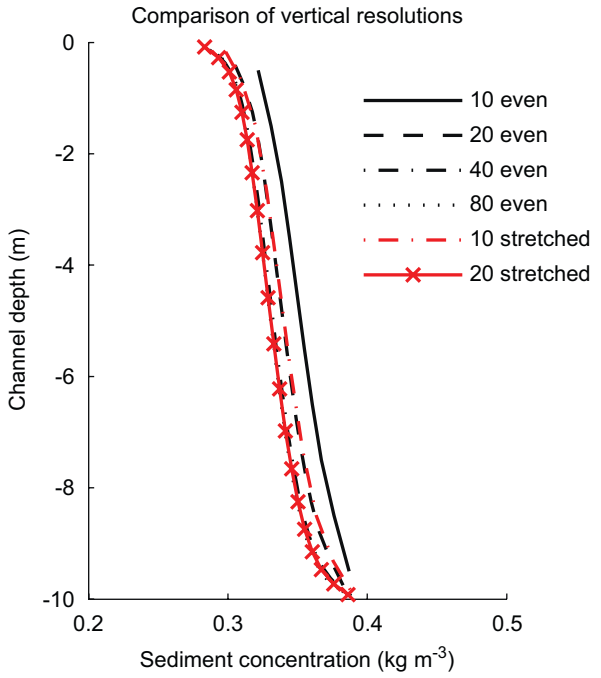

Fig. 3. Effect of vertical resolution on computed profiles of sediment concentration. Increasing the number of evenly distributed cells shows convergence to a steady profile. Simulation with 20 levels using increased boundary layer resolution is consistent with simulation using 80 evenly distributed layers.

The same profile can be obtained with 20 levels when the vertical stretching parameters are used to increase resolution near the bed (Fig. 3).

Simulations with different turbulence closures produce significantly different profiles of velocity, eddy diffusivity, and sediment concentration (Fig. 4). Results were obtained with the two-equation k-ε closure, the original Mellor and Yamada (1982) level 2.5 closure (MY25) and an analytical expression (ANA) obtained by stipulating a parabolic shape to the eddy viscosity profile:

$$K_M = \kappa u_* z\left(1-\frac{z}{D}\right) \tag{52}$$

where u_* is the friction velocity, z is the distance above the bed, and D is the water depth (10 m). The friction velocity is calculated by substituting the log law ($u(z)/u_* = 1/\kappa \ln(z/z_0)$) into the depth-mean flow equation and integrating over the entire depth of flow, yielding

$$u_* = \frac{\kappa\bar{u}}{\ln(D/z_0)-1+z_0/D} \tag{53}$$

where $\bar{u}$ is the depth-mean velocity, and parameters in Table 2 produce $u_* = 0.0625\,\mathrm{m\,s^{-1}}$. The eddy diffusivity in the model is determined from the turbulent Prandtl number (Pr; ratio of eddy viscosity/eddy diffusivity) and, for neutrally stable flow, $Pr = 0.39/0.49 = 0.80$ (Kantha and Clayson, 1994; Warner et al., 2005). Therefore the algebraic eddy diffusivity is $K_H = K_M/0.80$ (Table 3).

The slope of the free surface should equal the bottom slope in steady uniform open-channel flow, producing a momentum balance of

$$\tau/\rho = u_*^2 = g\frac{\partial\eta}{\partial x}D \tag{54}$$

This theoretical balance is $(0.0625\,\mathrm{m\,s^{-1}})^2 = (9.81\,\mathrm{m\,s^{-2}})(0.00004)(10\,\mathrm{m})$. The modeled balance depends on the calculated bottom shear stress and, therefore, on the details of the turbulence closure. The free-surface slopes generated using ANA and k–ε are very nearly equal to 4×10^{-5} so Eq. (54) holds with approximately the values calculated above. The slope calculated using the MY25 is closer to 3×10^{-5}, which balances u_* of $0.0544\,\mathrm{m^2\,s^{-2}}$. The reduced shear near the bed with MY25 is apparent in the velocity profiles and results in less mixing and lower sediment concentrations (Fig. 4). This behavior is a result of the wall function used in the original MY25 closure, but results consistent with ANA and k-ε can be obtained using the alternative wall function proposed by Blumberg et al. (1992); see Warner et al. (2005).

4.2. Example 2: Trench migration

This example tests the sediment-transport components of bedload (Meyer-Peter Müeller formulation),

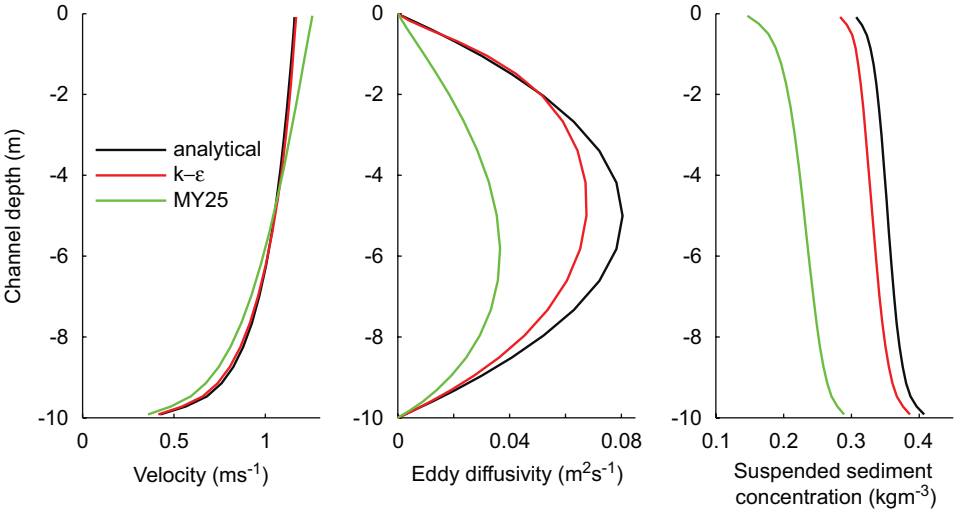

Fig. 4. Vertical profiles of velocity, eddy diffusivity, and sediment concentration for three of turbulence closure options of analytical parabolic expression, k–ε, and MY25. Simulations used 20 vertical stretched levels.

Table 3
Results for open-channel flow test case

	$\partial\eta/\partial x$	u^* ($m^2 s^{-2}$)
Calculated	4.00e−5	0.0625
ANA	4.21e−5	0.0643
k–ε	3.98e−5	0.0626
MY25	3.00e−5	0.0544

suspended-sediment load, and morphologic evolution by simulating the laboratory experiment of van Rijn (1987), also described in van Rijn (1993). The experimental and model setup (Table 4) consist of flow along a 30-m straight channel with a vertical depression (trench) incised in the mobile sand bed (Fig. 5). The bed material is well-sorted fine sand ($D_{50} = 140\,\mu m$). Flow is steady with a depth-mean velocity of $0.51\,m\,s^{-1}$. In the model simulations, flow and suspended-sediment are allowed to reach steady state before morphologic evolution is initiated, there is an unlimited supply of available sediment, and the k-e turbulence-closure model is used.

As the flow travels into the deeper water of the trench, flow velocity and bottom stress decrease. Sediment begins to settle out of suspension, and bedload transport converges, so sediment accumulates at the upstream end of the trench. At the downstream end of the trench, erosion occurs as depth decreases, flow accelerates, and transport diverges. The trench migrates in the direction of the flow (left to the right in Fig. 5) as the upstream end is filled, and the downstream end eroded.

Computed and observed velocity and suspended-sediment profiles at five locations, and the initial and final bed elevations are compared in Fig. 5. The velocity profiles are in good agreement with the measurements. The deceleration of near-bottom flow in the middle of the trench is captured well. Suspended-sediment profiles at the upstream and downstream ends match the observations but, in the trench, calculated concentrations of suspended-sediment deviate slightly from the observed profiles. At the end of the simulation, the modeled trench has migrated as far as the observed trench, but has not filled as much (compare red and blue lines in Fig. 5).

4.3. Example 3: Tidal inlet wave–current coupled system

This example demonstrates wave–current coupling and includes wave-induced forcing by the radiation-stress terms. The domain is a rectangular basin 15 km in width and 14 km long, with a uniform initial depth of 4 m (Table 5). The northern, western, and eastern edges are open with radiation boundary conditions. Along the center of the domain is a wall with a centered 2 km wide inlet. The model is forced by oscillating the water level on the northern edge with a tidal amplitude of 1 m. Waves are also imposed on the northern edge with a wave height of 1 m, directed to the south with a

period of 10 s. The model is run with two configurations: (1) one-way coupled with wave information passed to the circulation model and (2) two-way fully coupled. The model hydrodynamics were simulated for a period of 2 days with a morphologic scale factor of 10, simulating a 20-day period.

In the one-way coupled system, wave heights evolve to a steady state, decreasing southward toward the inlet and showing no effect from the inlet currents (Fig. 6). At the peak of the ebb tide the combined wave–current bottom stresses are maximum near the location of maximum currents. Bathymetric evolution produces a flood and a larger ebb shoal. By contrast, the two-way coupled model results show greatly increased wave heights in front of the inlet as the approaching wave interacts with an opposing current. The increased wave heights create combined bottom stresses that are greater than the one-way coupled system, and the peak bottom stresses are located near the maximum wave heights. The morphology evolves a stronger ebb shoal due to the higher stresses and the shoal is displaced slightly further seaward.

Table 4
Model parameters for test case 2—migrating trench

Model parameter	Variable	Value
Length, width, depth	*Xsize*, *Esize*, *depth*	30, 0.5, 0.39 m
Number of grid spacings	*Lm*, *Mm*, *Nm*	300, 4, 20
Bottom roughness	*Zob*	0.000833 m
Time step	*dt*	0.05 s
Simulation steps	*Ntimes*	30 000 initial (no morphology), 12000 with morphology
Morphology factor	*morph_fac*	0 for initial, 90 for morph
Settle velocity	w_s	$11.0\,\mathrm{mm\,s^{-1}}$
Erosion rate	E_0	$0.35\times10^{-2}\,\mathrm{kg\,m^{-2}\,s^{-1}}$
Critical stresses	τ_{cd}, τ_{ce}	$0.11\,\mathrm{N\,m^{-2}}$
Porosity	φ	0.40
Bed slope	S_0	4×10^{-4}
Inflow/outflow boundary condition	$\bar{u}$	$0.51\,\mathrm{m\,s^{-1}}$

4.4. Example 4: Evolution of surficial sediment distribution in Massachusetts Bay

Here we highlight the sediment-transport capabilities of the model and its ability to simulate the transport of a mixed grain size bed and the evolution of the sea floor sediment grain size distribution. A detailed description is provided in Warner et al. (in press). In this simulation the sediment bed was initialized with 10 vertical levels with the top 6 layers at 0.01 m thick and the bottom 4 at 0.10 m thick. All layers had a porosity of 0.50 and initial spatially-uniform distributions of sediments with 7 equal fractions of grain size ranging from 7 phi (fine silt) to 1 phi (coarse sand) with

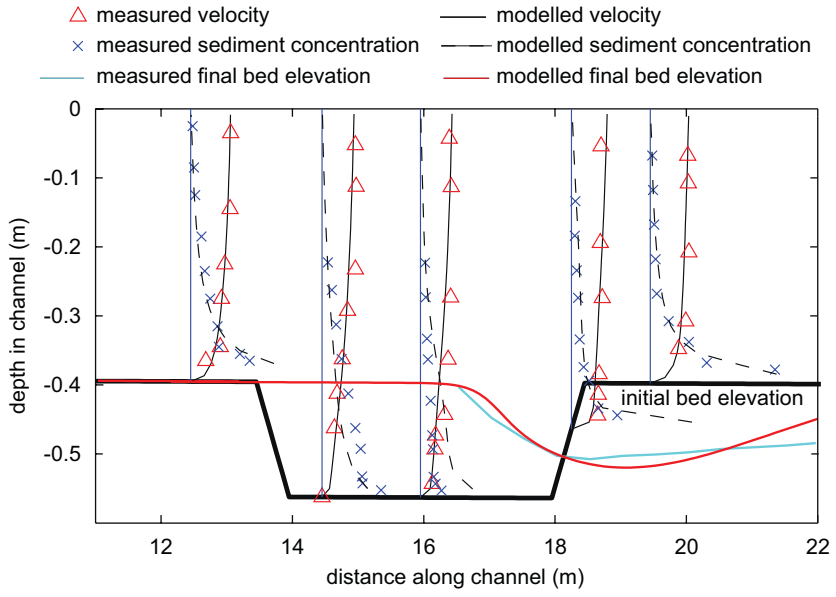

Fig. 5. Migrating trench test case showing initial (black line), final measured (cyan), and final modeled (red) bed elevations. Vertical profiles of measured and modeled suspended-sediment concentration and velocity are compared.

Table 5
Model parameters for test case 3—tidal inlet

Model parameter	Variable	Value
Length, width, depth	*Xsize*, *Esize*, *depth*	15,000, 14,000, 4.0 m
Number of grid spacings	*Lm*, *Mm*, *Nm*	75, 70, 10
Bottom roughness	z_{ob}	0.015 m
Time step	*dt*	10 s
Simulation steps	*Ntimes*	17280 steps (2 day)
Morphology factor	*morph_fac*	10 (= 20 day scaled simulation)
Settle velocity	w_s	$11.0\,\mathrm{mm\,s^{-1}}$
Erosion rate	E_0	$5\times10^{-3}\,\mathrm{kg\,m^{-2}\,s^{-1}}$
Critical stresses	τ_{cd}, τ_{ce}	$0.10\,\mathrm{N\,m^{-2}}$
Porosity	φ	0.50
Bed thickness	*bed_thick*	10.0 m
Northern edge tide	A, T_t	1.0 m, 12 h
Northern edge wave height	H_{sig}	2 m
Northern edge wave period	T	10 s
Northern edge wave direction	θ	From 0°

critical shear stresses ranging from 0.022 to 0.27 Pa respectively. The simulation had a tidal forcing with 7 main constituents along the open boundary. After a spin-up time period, forcing with realistic wind stress and wave fields were imposed to simulate an 8-day December 1992 storm. This storm was repeated 10 times with an intervening 1-day period to allow sediment to settle out of the water column. The model time step was 30 seconds and hourly results were saved.

The repeating storm simulation generated realistic patterns of bottom stress, sediment resuspension, and bathymetric change (Fig. 7). The instantaneous bottom stress (maximum combined wave/current) at the peak of storm activity is greatest in the shallow water along the coastline and on the crest of Stellwagen Bank, coinciding with locations of increased bottom orbital velocities from the wave model (Fig. 7). Stresses are lower in Stellwagen Basin where the near-bottom wave currents are attenuated in the deep water, and in Cape Cod Bay because the Cape shelters the Bay from waves from the northeast. Along the western shore of

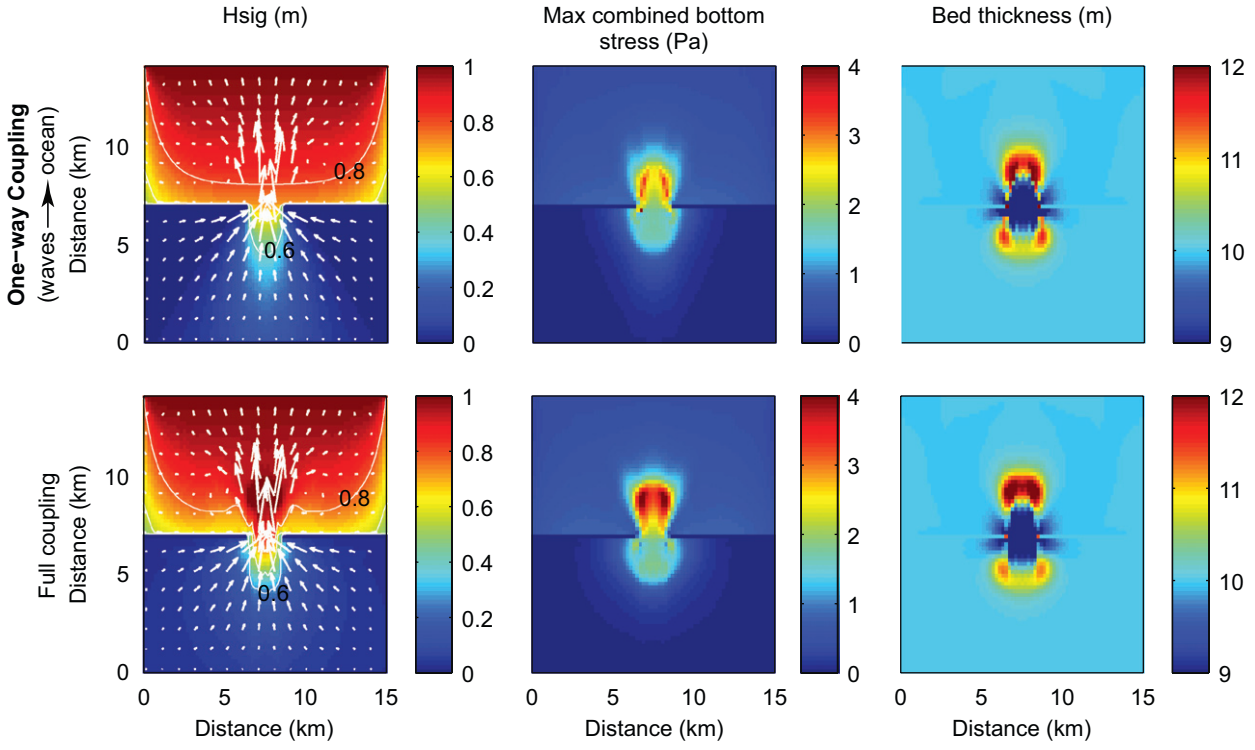

Fig. 6. Tidal inlet test case. Comparison of significant wave height, bottom stress, and bed thickness for a one-way coupled simulation (wave parameters sent to ocean model) to a fully coupled simulation (wave parameters to ocean model and ocean data to wave model). See text for full data transfer description. For the fully coupled system, wave heights show effect of currents, maximum bottom stress in enhanced due to increased wave heights, and bed thickness develops a stronger flood shoal than the one-way coupled system.

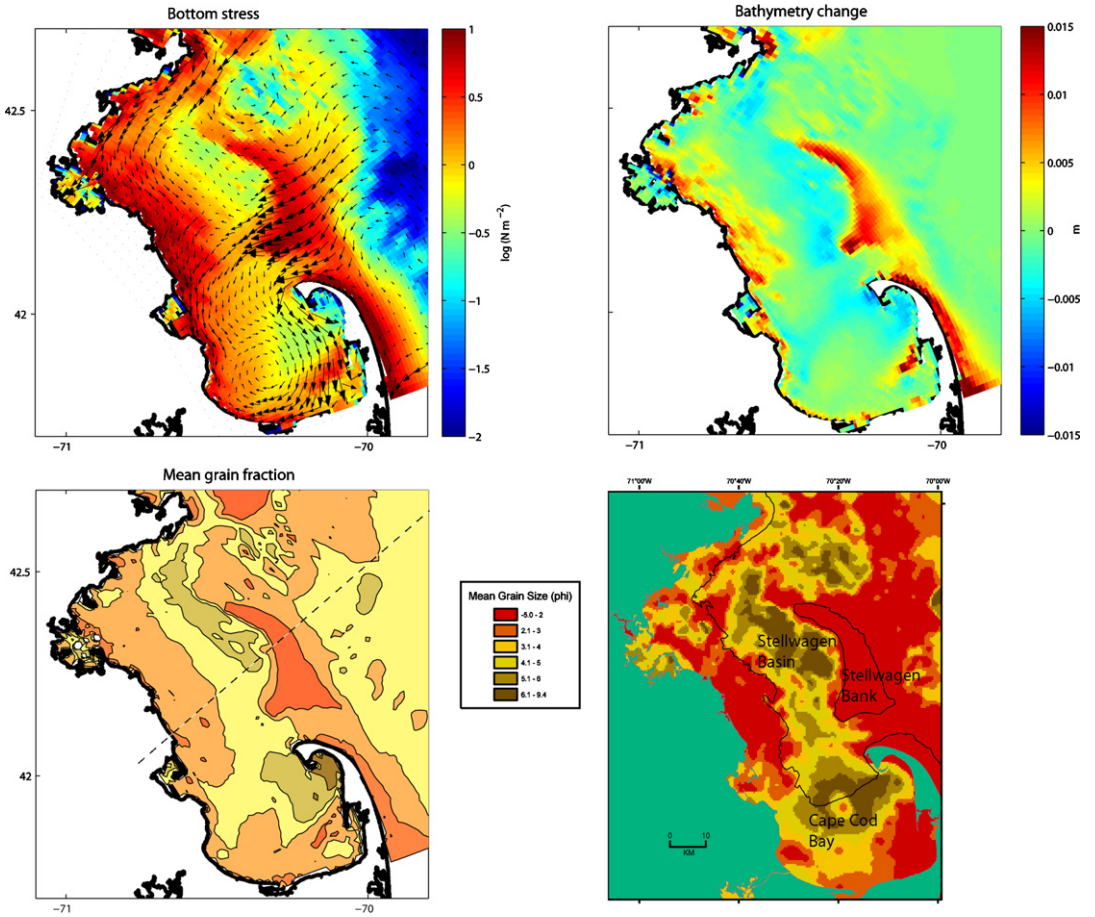

Fig. 7. Results from model simulation of Massachusetts Bay for the evolution of a mixed sediment bed in response to a sequence of 10 idealized northeast storms, modeled after the December 1992 storm with winds from 50°. Panels show instantaneous wave–current bottom stress at peak of storm (A), and change in bathymetry (B) and final mean surficial grain size (C) following the 10-storm sequence. The observed surficial grain size distribution (D) qualitatively matches the evolved sediment texture.

Massachusetts Bay (in the region opposite of Stellwagen Basin) the combined wave and current stress is high but then decreases between Plymouth and Barnstable. The instantaneous suspended-sediment concentrations during the storm (not shown) are greatest in the regions of highest stress and are lowest in Cape Cod Bay and in Stellwagen Basin. At the end of the simulation, net erosion has occurred along the crest of Stellwagen Bank, along the western shore of Massachusetts Bay (in the region of high stress), and along the outer arm of Cape Cod, reaching maximum values of 0.02 m (Fig. 7b). Deposition occurs in Stellwagen Basin immediately west of Stellwagen Bank, and in Cape Cod Bay.

The surficial grain size distribution after 10 storms (Fig. 7C) has approached a steady-state, with continued small changes that do not significantly alter the pattern described here. The sediment texture is coarser in regions of high stress and finer in areas of low stress. The surficial sediment texture qualitatively resembles the observed distribution (Fig. 7d; Poppe et al., 2003). The crest of Stellwagen Bank, the outer Cape, and the western shore of Massachusetts Bay north of Plymouth have been winnowed to sizes of 2–3φ and sediment deposition in Cape Cod Bay and Stellwagen Basin has produced a surface of 5–6φ material. The material east of Stellwagen Bank is slightly finer in the model, possibly because the Gulf of Maine coastal current which could transport the 4 and 5φ material further to the south is not simulated.

5. Future work

Future model improvements will be implemented using an open-source, community development approach. We plan to investigate alternative approaches

to wave-induced circulation in the nearshore, including the vortex-force representation of McWilliams et al. (2004). We also are investigating other model-coupling methodologies, such as the Earth System Modeling Framework (ESMF, http://www.esmf.ucar.edu/). Algorithms to represent cohesive sediment behavior and biodiffusive mixing are under development. Several aspects of the BBL calculations will be improved by including effects of sediment-induced stratification, time-dependent ripple evolution, and representation of bedforms that develop under combinations of waves and currents. These processes and others are currently being investigated.

6. Conclusions

We are developing a coupled wave–current-sediment transport-morphodynamic oceanographic circulation model applicable to studies in rivers, lakes, estuaries, coastal environments, and the coastal ocean. The ocean circulation model ROMS has been coupled using the MCT to the surface wave model SWAN. We have incorporated nearshore radiation-stress terms and a surface roller model to account for surfzone (nearshore) processes. The sediment-transport algorithms have been implemented to transport an unlimited number of user-defined sediment classes. Suspended-sediment transport is computed with the advection–diffusion equation and a vertical-settling algorithm not restricted by the CFL criteria. Erosion and deposition algorithms control mass balance between suspended sediment in the water column and the evolution of a multi-level bed framework. The bed tracks the mass, fractions, thickness, and surface properties of the sediment and thus allows computations of morphological behavior and stratigraphy. Bedload transport occurs in the top layer for all the sediment classes. Additional features are being implemented to account for such conditions as mixed grain sizes, cohesive behavior, and bed biodiffusivity.

The model in its current state (ROMS 3.0) is available online and model development is being conducted as an open-source community effort. We hope for feedback that will add features and make the model more robust as the community of users and developers grows.

Acknowledgments

This work has been supported by the US Geological Survey Coastal and Marine Geology Program and by the Office of Naval Research EuroSTRATAFORM project. We thank the reviewers for their comments and the developers of ROMS for open access to their code.

References

Arakawa, A., 1966. Computational design for long-term numerical integration of the equations of fluid motion: Two-dimensional incompressible flow. Part I. Journal of Computational Physics 1, 119–143.

Ariathurai, C.R., Arulanandan, K., 1978. Erosion rates of cohesive soils. Journal of Hydraulics Division 104 (2), 279–282.

Blaas, M., Dong, C., Marchesiello, P., McWilliams, J.C., Stolzenbach, K.D., 2005. Sediment-transport modeling on Southern Californian Shelves: a ROMS case study. Continental Shelf Research 27, 832–853.

Blumberg, A.F., Galperin, B., O'Connor, D.J., 1992. Modeling vertical structure of open-channel flows. Journal of Hydraulic Engineering, ASCE 118 (H8), 1119–1134.

Booij, N., Ris, R.C., Holthuijsen, L.H., 1999. A third-generation wave model for coastal regions, Part I, Model description and validation. Journal of Geophysical Research 104 (C4), 7649–7666.

Booij, N., Haagsma, I.J.G., Holthuijsen, L.H., Kieftenburg, A.T.M.M., Ris, R.C., van der Westhuysen, A.J., Zijlema, M., 2004. SWAN Cycle III version 40.41 User Manual. Delft University of Technology.

Casulli, V., Cheng, R., 1992. Semi-implicit finite difference methods for three-dimensional shallow water flow. International Journal for Numerical Methods in Fluids 15, 629–648.

Chassignet, E.P., Arango, H.G., Dietrich, D., Ezer, T., Ghil, M., Haidvogel, D.B., Ma, C.-C., Mehra, A., Paiva, A.M., Sirkes, Z., 2000. DAMEE-NAB: the base experiments. Dynamics of Atmospheres and Oceans 32, 155–183.

Colella, P., Woodward, P., 1984. The piecewise parabolic method (PPM) for gas-dynamical simulations. Journal of Computational Physics 54, 174–201.

Durski, S.M., Glenn, S.M., Haidvogel, D.B., 2004. Vertical mixing schemes in the coastal ocean: comparison of the level 2.5 Mellor-Yamada scheme with an enhanced version of the K profile parameterization. Journal of Geophysical Research 109, C01015.

Fredsøe, J., Deigaard, R., 1992. Mechanics of coastal sediment transport. In: Liu, P.P.L.-F. (Ed.), Advanced Series on Ocean Engineering, Vol. 3. World Scientific, Singapore, p. 392.

Grant, W.D., Madsen, O.S., 1979. Combined wave and current interaction with a rough bottom. Journal of Geophysical Research 84 (C4), 1797–1808.

Grant, W.D., Madsen, O.S., 1982. Movable bed roughness in unsteady oscillatory flow. Journal Geophysical Research 87 (C1), 469–481.

Haidvogel, D.B., Arango, H.G., Hedstrom, K., Beckmann, A., Malanotte-Rizzoli, P., Shchepetkin, A.F., 2000. Model evaluation experiments in the North Atlantic Basin: Simulations in nonlinear terrain-following coordinates. Dynamics of Atmospheres and Oceans 32, 239–281.

Haidvogel, D.B., Arango, H.G., Budgell, W.P., Cornuelle, B.D., Curchitser, E., Di Lorenzo, E., Fennel, K., Geyer, W.R., Hermann, A.J., Lanerolle, L., Levin, J., McWilliams, J.C.,

Miller, A.J., Moore, A.M., Powell, T.M., Shchepetkin, A.F., Sherwood, C.R., Signell, R.P., Warner, J.C., Wilkin, J., 2007. Regional Ocean forecasting in terrain-following coordinates: model formulation and skill assessment. Journal of Computational Physics.

Harris, C.K., Wiberg, P.L., 1997. Approaches to quantifying long-term continental shelf sediment transport with an example from the northern California STRESS mid-shelf site. Continental Shelf Research 17, 1389–1418.

Harris, C.K., Wiberg, P.L., 2001. A two-dimensional, time-dependent model of suspended sediment transport and bed reworking for continental shelves. Computers & Geosciences 27, 675–690.

Jacob, R., Larson, J., Ong, E., 2005. M x N Communication and parallel interpolation in community climate system model version 3 using the model coupling toolkit. International Journal of High Performance Computing Applications 19 (3), 293–307.

Jonsson, I.C., Carlsen, N.A., 1976. Experimental and theoretical investigations in an oscillatory boundary layer. Journal of Hydraulic Research, ASCE 14 (1), 45–60.

Kantha, L.H., Clayson, C.A., 1994. An improved mixed layer model for geophysical applications. Journal of Geophysical Research 99 (C12), 25,235–25,266.

Large, W.G., McWilliams, J.C., Doney, S.C., 1994. A review and model with a nonlocal boundary layer parameterization. Reviews of Geophysics 32, 363–403.

Larson, J., Jacob, R., Ong, E., 2005. The model coupling toolkit: a new fortran90 toolkit for building multiphysics parallel coupled models. International Journal of High Performance Computing Applications 8 (19), 277–292.

Lesser, G.R., Roelvink, J.A., van Kester, J.A.T.M., Stelling, G.S., 2004. Development and validation of a three-dimensional morphological model. Coastal Engineering 51, 883–915.

Li, M.Z., Amos, C.L., 2001. SEDTRANS96: the upgraded and better calibrated sediment-transport model for continental shelves. Computers & Geosciences 27, 619–645.

Li, M., Zhong, L., Boicourt, B., 2005. Simulation of Chesapeake Bay Estuary: sensitivity to turbulence mixing parameterizations and comparison with hydrographic observations. Journal of Geophysical Research 110, C12004.

Liu, X.-D., Osher, S., Chan, T., 1994. Weighted essentially non-oscillatory schemes. Journal of Computational Physics 115, 200–212.

Madsen, O.S., 1994. Spectral wave–current bottom boundary layer flows. In: Coastal Engineering 1994. Proceedings of the 24th International Conference on Coastal Engineering Research Council, Kobe, Japan, pp. 384–398.

Malarkey, J., Davies, A.G., 2003. A non-iterative procedure for the Wiberg and Harris (1994) oscillatory sand ripple predictor. Journal of Coastal Research 19 (3), 738–739.

McWilliams, J.C., Restrepo, J.M., Lane, E.M., 2004. An asymptotic theory for the interaction of waves and currents in coastal waters. Journal of Fluid Mechanics 511, 135–178.

Mellor, G.L., 2003. The three-dimensional current and surface wave equations. Journal of Physical Oceanography 33, 1978–1989.

Mellor, G.L., 2005. Some consequences of the three-dimensional currents and surface wave equations. Journal of Physical Oceanography 35, 2291–2298.

Mellor, G.L., Yamada, T., 1982. Development of a turbulence closure model for geophysical fluid problems. Reviews of Geophysics and Space Physics 20, 851–875.

Meyer-Peter, E., Müeller, R., 1948. Formulas for bedload transport. In: Report on the 2nd Meeting International Association Hydraulic Structure Research. Stockholm, Sweden, pp. 39–64.

Nielsen, P., 1986. Suspended sediment concentrations under waves. Coastal Engineering 10, 23–31.

Nielsen, P., 1992. Coastal Bottom Boundary Layers and Sediment Transport. Advanced Series on Ocean Engineering, vol. 4. World Scientific, Singapore, 324pp.

Phillips, O.M., 1969. The Dynamics of the Upper Ocean. Cambridge Press, Cambridge.

Poppe, L.J., Paskevich, V.F., Williams, S.J., Hastings, M.E., Kelly, J.T., Belknap, D.F., Ward, L.G., FitzGerald, D.M., Larsen, P.F., 2003. Surficial sediment data from the Gulf of Maine, Georges Bank, and vicinity: A GIS Compilation. US Geological Survey Open-File Report 03-001, 〈http://pubs.usgs.gov/of/2003/of03-001/index.htm〉.

Roelvink, J.A., 2006. Coastal morphodynamic evolution techniques. Coastal Engineering 53, 277–287.

Shchepetkin, A.F., McWilliams, J.C., 2005. The regional ocean modeling system (ROMS): a split-explicit, free-surface, topography-following-coordinates ocean model. Ocean Modelling 9, 347–404.

Sherwood, C.R., Harris, C.K., Geyer, W.R., Butman, B., 2002. Toward a community coastal sediment-transport modeling system: Report of the Second Workshop. EOS, Transactions, American Geophysical Union 83 (51).

Smith, J.D., 1977. Modeling of sediment transport on continental shelves. In: Goldberg, E.D., McCave, I.N., O'Brien, J.J., Steele, J.H. (Eds.), The Sea, Vol. 6. Wiley-Interscience, New York, pp. 539–577.

Smith, J.D., McLean, S.R., 1977. Spatially averaged flow over a wavy surface. Journal of Geophysical Research 82 (12), 1735–1746.

Soulsby, R.L., 1995. Bed shear-stresses due to combined waves and currents. In: Stive, M.J.F. (Ed.), Advances in Coastal Morphodynamics: An Overview of the G8-Coastal Morphodynamics Project, Co-Sponsored by the Commission of The European Communities Directorate General XII pp. 4.20–4.23.

Soulsby, R.L., 1997. Dynamics of Marine Sands. Thomas Telford, London, 249pp.

Soulsby, R.L., Damgaard, J.S., 2005. Bedload sediment transport in coastal waters. Coastal Engineering 52 (8), 673–689.

Styles, R., Glenn, S.M., 2000. Modeling stratified wave and current bottom boundary layers on the continental shelf. Journal of Geophysical Research 105 (C10), 24,119–24,139.

Styles, R., Glenn, S.M., 2002. Modeling bottom roughness in the presence of wave-generated ripples. Journal of Geophysical Research 107 (C8), 24/1–24/15.

Svendsen, I.A., 1984. Wave heights and set-up in a surf zone. Coastal Engineering 8, 303–329.

Svendsen, I.A., Haas, K., Zhao, Q., 2002. Quasi-3D nearshore circulation model SHORECIRC, User's Manual, Draft Report, Center for Applied Coastal Research, Department of Civil Engineering, University of Delaware, Newark.

Umlauf, L., Burchard, H., 2003. A generic length-scale equation for geophysical turbulence models. Journal of Marine Research 61, 235–265.

van Rijn, L.C., 1987. Mathematical modelling of morphological processes in the case of suspended sediment transport. Delft Technical University, Delft Hydraulics Communication No. 382, Delft, The Netherlands.

van Rijn, L.C., 1993. Principles of Sediment Transport in Rivers, Estuaries, and Coastal Seas. Aqua Publications–I11, Amsterdam, The Netherlands, 614pp.

Warner, J.C., Sherwood, C.R., Arango, H.G., Signell, R.P., 2005. Performance of four turbulence closure models implemented using a generic length scale method. Ocean Modelling 8, 81–113.

Warner, J.C., Perlin, N., Skyllingstad, E. (in press). Using the model coupling toolkit to couple earth system models. Environmental Modelling and Software.

Wiberg, P.L., Harris, C.K., 1994. Ripple geometry in wave-dominated environments. Journal of Geophysical Research 99 (C1), 775–789.

Wiberg, P.L., Nelson, J.M., 1992. Unidirectional flow over asymmetric and symmetric ripples. Journal of Geophysical Research 97 (C8), 12,745–12,761.

Wiberg, P.L., Rubin, D.M., 1989. Bed roughness produced by saltating sediment. Journal of Geophysical Research 94 (C4), 5011–5016.

Wiberg, P.L., Sherwood, C.R. (this issue). Calculating wave-generated bottom orbital velocity from surface wave parameters. Computers & Geosciences, doi:10.1016/j.cageo.2008.02.010.

Wijesekera, H.W., Allen, J.S., Newberger, P.A., 2003. Modeling study of turbulent mixing over the continental shelf: comparison of turbulent closure schemes. Journal of Geophysical Research 108 (C3), 3103.